

Structure and transport properties of $HoNiO_3$ under high pressure

Liyan Wang(汪礼艳), Di Peng(彭帝), Yuchen Cui(崔雨晨), Yiming Wang(王弈铭), Jingxin Gao(高景鑫), Tao Luo(罗涛), Zhikai Zhu(朱智凯), Kejun Bu(卜克军), Yuzhu Wang(王玉柱), Sibo Zhan(展思博), Jikun Chen(陈吉堃), Huaqing Xie(谢华清), Zihua Wu(吴子华), Hongliang Dong(董洪亮), and Zhidan Zeng(曾徵丹)

Citation: Chin. Phys. B, 2026, 35 (**5**): 057103. DOI: 10.1088/1674-1056/ae3c92
http://cpb.iphy.ac.cn; http://iopscience.iop.org/cpb

What follows is a list of articles you may be interested in

Single crystal growth and electronic structure of Fe-doped $Sr_3Ir_2O_7$

Muhammad Waqas, Bingqian Wang(王冰倩), Shuting Peng(彭舒婷), Jianchang Shen(沈建昌), Linwei Huai(淮琳崴), Xiupeng Sun(孙秀鹏), Yu Miao(缪宇), Pelda Uzun, Runqing Luan(栾润青), Zikun Feng(冯梓琨), Dai Pan(潘岱), Xinru Yong(勇欣茹), Hongxu Sun(孙鸿绪), Zhipeng Ou(欧志鹏), and Junfeng He(何俊峰)

Chin. Phys. B, 2025, 34 (**10**): 107101. DOI: 10.1088/1674-1056/adda0b

Insights to unusual antiferromagnetic behavior and exchange coupling interactions in $Mn_{23}C_6$

Ze-Kun Yu(于泽坤), Chao Zhou(周超), Kuo Bao(包括), Zhao-Qing Wang(王兆卿), En-Xuan Li(李恩萱), Jin-Ming Zhu(朱金铭), Yuan Qin(秦源), Yu-Han Meng(孟钰涵), Pin-Wen Zhu(朱品文), Qiang Tao(陶强), and Tian Cui(崔田)

Chin. Phys. B, 2025, 34 (**3**): 037101. DOI: 10.1088/1674-1056/adaadd

Unveiling the pressure-driven metal-semiconductor-metal transition in the doped TiS_2

Jiajun Chen(陈佳骏), Xindeng Lv(吕心邓), Simin Li(李思敏), Yaqian Dan(但雅倩), Yanping Huang(黄艳萍), and Tian Cui(崔田)

Chin. Phys. B, 2024, 33 (**6**): 067104. DOI: 10.1088/1674-1056/ad4325

Single crystal growth and electronic structure of Rh-doped $Sr_3Ir_2O_7$

Bingqian Wang(王冰倩), Shuting Peng(彭舒婷), Zhipeng Ou(欧志鹏), Yuchen Wang(王宇晨), Muhammad Waqas, Yang Luo(罗洋), Zhiyuan Wei(魏志远), Linwei Huai(淮琳崴), Jianchang Shen(沈建昌), Yu Miao(缪宇), Xiupeng Sun(孙秀鹏), Yuewei Yin(殷月伟), and Junfeng He(何俊峰)

Chin. Phys. B, 2023, 32 (**8**): 087108. DOI: 10.1088/1674-1056/acd7d5

Anisotropic thermoelectric transport properties in polycrystalline $SnSe_2$

Caiyun Li(李彩云), Wenke He(何文科), Dongyang Wang(王东洋), and Li-Dong Zhao(赵立东)

Chin. Phys. B, 2021, 30 (**6**): 067101. DOI: 10.1088/1674-1056/abeee1

SPECIAL TOPIC — Structures and properties of materials under high pressure

Structure and transport properties of $HoNiO_3$ under high pressure

Liyan Wang(汪礼艳)[1,2], Di Peng(彭帝)[2], Yuchen Cui(崔雨晨)[3], Yiming Wang(王弈铭)[2], Jingxin Gao(高景鑫)[3], Tao Luo(罗涛)[2], Zhikai Zhu(朱智凯)[2], Kejun Bu(卜克军)[2], Yuzhu Wang(王玉柱)[4], Sibo Zhan(展思博)[5], Jikun Chen(陈吉堃)[3], Huaqing Xie(谢华清)[1], Zihua Wu(吴子华)[1,†], Hongliang Dong(董洪亮)[2,‡], and Zhidan Zeng(曾徵丹)[2]

[1] *School of Energy and Materials, Shanghai Polytechnic University, Shanghai* 201209, *China*
[2] *Center for High Pressure Science and Technology Advanced Research, Shanghai* 201203, *China*
[3] *School of Materials Science and Engineering, University of Science and Technology Beijing, Beijing* 100083, *China*
[4] *Shanghai Synchrotron Radiation Facility, Shanghai Advanced Research Institute, Chinese Academy of Sciences, Shanghai* 201204, *China*
[5] *Analysis Center of Agrobiology and Environmental Sciences, Faculty of Agriculture, Life and Environment Sciences, Hangzhou* 310058, *China*

(Received 2 January 2026; revised manuscript received 7 January 2026; accepted manuscript online 23 January 2026)

Rare-earth nickelate (ReNiO$_3$, with $Re \neq$ La) constitutes a paradigmatic class of strongly correlated electron systems, exhibiting a remarkable tunability of the metal–insulator transition (MIT) in response to external stimuli such as hydrostatic pressure, temperature, and chemical doping. This tunability arises from the competitive interplay among charge, spin, and orbital degrees of freedom. However, the fundamental mechanisms governing the effective control of the MIT under extreme conditions, particularly the intricate coupling between lattice dynamics and electronic localization, remain elusive. This knowledge gap poses a significant challenge to both fundamental research and practical applications of these materials. Herein, we present a systematic investigation of the structural phase transitions and electrical transport properties of $HoNiO_3$ under extreme conditions. In situ high-pressure x-ray diffraction (XRD) analysis uncovers a structural evolution pathway: an initial transition from a monoclinic insulating phase ($P2_1/n$) to an orthorhombic metallic phase ($Pbnm$) at approximately 17 GPa, followed by the emergence of a mixed-phase region ($Pbnm$ and $R\bar{3}c$) at approximately 35 GPa. Complementary electrical transport measurements reveal a pronounced sensitivity of the metal–insulator transition temperature (T_{MIT}) to the synergistic effects of high pressure and low temperature. These findings not only provide crucial experimental evidence for elucidating the structure–property relationship in $HoNiO_3$ under extreme conditions, but also lay a conceptual foundation for designing advanced functional devices based on ReNiO$_3$ materials, with promising applications in high-sensitivity pressure sensors and temperature-responsive switches featuring tunable activation thresholds.

Keywords: metal–insulator transition (MIT), electrical transport properties, high pressure, x-ray diffraction (XRD)

PACS: 71.30.+h, 74.25.F−, 07.35.+k, 61.05.cp

DOI: 10.1088/1674-1056/ae3c92 **CSTR:** 32038.14.CPB.ae3c92

1. Introduction

The perovskite oxides ReNiO$_3$ have recently attracted growing interest in condensed matter physics and functional materials science, owing to their intriguing electronic structures featuring strongly localized 3d orbitals and the resulting exotic physical properties.[1–3] $SmNiO_3$, for instance, exhibits unique weak electric-field sensing capabilities in seawater environments, providing a novel material platform for underwater electric-field detection technologies with enhanced stability.[4,5] However, there remains a critical research gap in ReNiO$_3$-based device applications, particularly regarding systematic investigations of their metal–insulator transition (MIT) under extreme conditions, which are essential for deep-sea adaptation and anisotropic charge transport behavior.[6,7] The complex interplay among lattice, charge, and orbital degrees of freedom under non-equilibrium conditions hinders the understanding of the crystalline structure evolution of ReNiO$_3$, thereby impeding a comprehensive understanding of their pressure-sensitive behaviors, precise performance modulation through atomic-scale engineering, and rational design of functional devices for extreme-environment applications.[8–10]

Application of external pressure enables the stabilization of non-equilibrium states of perovskite oxides by reducing their atomic bond lengths, which dramatically enhances electron–electron correlations and modifies orbital hybridization strength. These collective effects cooperatively drive a series of well-defined structural phase transitions, accompanied by distinct electronic property modulations.[11] The structural phase transitions in ReNiO$_3$ are accompanied by valence state changes of Ni ions, arising from charge redistribution and orbital-selective electron transfer.[12] This electronic reorganization induces band overlap between the valence and con-

†Corresponding author. E-mail: wuzihua@sspu.edu.cn
‡Corresponding author. E-mail: hongliang.dong@hpstar.ac.cn

© 2026 Chinese Physical Society and IOP Publishing Ltd. All rights, including for text and data mining, AI training, and similar technologies, are reserved.

duction bands, driving an insulator-to-metal transition through progressive collapse of the charge gap.[13–15] It is noteworthy that Kondo insulators are predominantly realized in rare-earth-based compounds, which exhibit correlated metallic behavior in the high-temperature regime due to partial screening of local moments.[16] The ReNiO$_3$ (Re = Pr, Nd, Sm, …, Eu) series undergoes a structural phase transition from orthorhombic (*Pbnm*) to rhombohedral ($R\bar{3}c$) symmetry under hydrostatic pressure.[12,17–22] Notably, EuNiO$_3$ exhibits this orthorhombic-to-rhombohedral transition at pressures exceeding 30 GPa.[18,19,23,24] In contrast, HoNiO$_3$ undergoes a monoclinic-to-orthorhombic phase transition at $T_{\mathrm{MIT}} = 583$ K, with no rhombohedral phase transition reported to date.[25,26]

Compared to conventional semiconductor devices, these oxide-based systems exhibit superior functional versatility and possess inherent advantages for future nanoscale miniaturization, including enhanced electron correlation effects and atomic-scale structural adaptability.[27] To address this, we integrate diamond anvil cell (DAC) technology with synchrotron-based *in situ* x-ray diffraction (XRD) and four-probe resistivity measurements, enabling direct observation of pressure-induced crystalline evolution and concurrent electronic transport changes.[28,29] A systematic investigation of the phase transition behavior in HoNiO$_3$ across distinct pressure regimes provides crucial insights into the intrinsic correlation between crystalline structure evolution and MIT characteristics at the atomic level. These findings offer new perspectives for understanding the fundamental physics of strongly correlated electron systems through combined structural and electronic probes.[30] The scientific significance of this work is manifested in three key aspects: (1) Our systematic investigation of HoNiO$_3$'s MIT under extreme pressure conditions provides the first comprehensive phase diagram for this prototypical correlated oxide, addressing a longstanding gap in high-pressure condensed matter physics. (2) We establish structure–property relationships between lanthanide ionic radius, oxygen octahedral distortions, and electronic phase transitions, advancing the fundamental understanding of rare-earth tuning in quantum materials. (3) The discovery of abrupt resistivity switching and anomalous thermal responses under pressure reveals promising applications in next-generation threshold-type piezoresistive sensors and thermally activated electronic devices, creating new avenues for functional oxide electronics.

2. Experimental methods

2.1. Synthesis method

HoNiO$_3$ rare-earth nickelate powders were synthesized via a eutectic molten salt-assisted heterogeneous precipitation (EMSHP) method. Stoichiometric precursors of Ho_2O_3 and NiO in a molar ratio of 1:2 were dissolved in a KCl–LiCl molten salt mixture. The eutectic composition of KCl and LiCl at a 4:6 molar ratio effectively lowered the melting point of the salt system. The reaction was conducted at temperatures ranging from 500 °C to 800 °C under an oxygen pressure of 15 MPa for 12 h. Subsequently, the melt was slowly cooled to room temperature to facilitate powder crystallization, followed by repeated rinsing with deionized water under ultrasonication to remove residual KCl and LiCl salts. The as-obtained powders were uniaxially cold-pressed into green pellets and subjected to a secondary annealing process under identical temperature and pressure conditions to enhance crystallinity for subsequent characterization.[31]

2.2. Sample characterizations

The ambient-pressure XRD patterns were acquired on beamline BL17UM at the Shanghai Synchrotron Radiation Facility (SSRF) using a monochromatic x-ray beam with a wavelength of 0.6209 Å. Ambient-pressure scanning electron microscopy (SEM) characterization was performed at the High Pressure Science and Technology Advanced Research Center (HPSTAR), where energy-dispersive x-ray spectroscopy (EDS) was employed for quantitative elemental composition analysis using an FEI Versa 3D system. High-pressure XRD measurements were performed at the BL17UM station of SSRF using a monochromatic x-ray beam with a wavelength of 0.4834 Å. The HoNiO$_3$ sample was loaded into a DAC sample chamber together with a ruby sphere for pressure calibration, while neon was employed as a quasi-hydrostatic pressure-transmitting medium. All two-dimensional XRD patterns were collected in transmission geometry and subsequently processed using the Dioptas software package for data integration and analysis,[32] with particular attention paid to the elimination of diamond anvil diffraction interferences during data reduction. The unit cell volume (V) was determined from high-pressure XRD data using the GSAS-II software package for Rietveld refinement. The interplanar spacing ratio (d/d_0) was derived through detailed analysis of the XRD diffraction patterns, where individual Bragg reflections were precisely fitted using PeakFit software with pseudo-Voigt functions to account for instrumental broadening effects. Both structural parameters were cross-verified through multiple refinement cycles to ensure consistency across the entire investigated pressure range.

High-pressure low-temperature electrical transport measurements were performed at HPSTAR using a physical property measurement system (PPMS, Quantum Design, USA). The four-probe method was employed for high-pressure transport characterization, with Pt wires serving as the electrodes. The DAC was utilized to apply hydrostatic pressure, enabling in situ resistance measurements as a function of pressure.

$HoNiO_3$ was loaded into the sample chamber of the DAC, which is composed of a mixture of cubic boron nitride and epoxy resin, with pressure calibration achieved through ruby fluorescence peak shifts. Specifically, four Pt wires were configured as electrodes and connected in a standard four-terminal geometry to minimize contact resistance. The DAC-mounted $HoNiO_3$ sample was then integrated with the PPMS for high-pressure low-temperature electrical transport studies.

3. Results and discussion

Figure 1(a) reveals that the polycrystalline $HoNiO_3$ sample consists of well-defined bulk grains with sizes around 3 μm, exhibiting sharp edges and smooth surfaces, which clearly demonstrate the high crystallinity of the as-prepared sample. As shown in Fig. 1(b), EDS analysis confirms the elemental ratio of Ho:Ni:O to be approximately 1:1:3, indicating the successful synthesis of the target material with the desired stoichiometry. Figure 1(c) displays the XRD pattern obtained at ambient pressure, which can be indexed to the monoclinic space group $P2_1/n$ (PDF#51-0395). The excellent agreement between the observed diffraction peaks and the Rietveld refinement profile further confirms the high purity and crystalline quality of the sample. The refined lattice parameters are determined to be $a = 5.1803(14)$ Å, $b = 5.4983(12)$ Å, $c = 7.4077(17)$ Å, and $\beta = 89.993(8)^\circ$.

To investigate the structural phase transition behavior of $HoNiO_3$ under GPa-level pressures, we have conducted high-pressure XRD measurements using a DAC.[33,34] Figure 2(a) reveals the structural evolution of $HoNiO_3$ under pressure. At ambient conditions, the compound crystallizes in the insulating $P2_1/n$ phase with low symmetry. Upon compression, all diffraction peaks exhibit pronounced right shifts, indicating substantial lattice compression. Concurrently, the systematic disappearance and merging of subsidiary peaks demonstrate a pressure-induced symmetry enhancement, suggesting a progressive structural transition toward higher-symmetry phases.[31,35] Owing to strong correlation effects among multiple electronic degrees of freedom, $ReNiO_3$ exhibits remarkably rich physical properties, including a pressure-tunable MIT that can be triggered at room temperature through lattice modification and bandwidth control.[36,37] At a critical pressure of 16.9 GPa, the system undergoes a complete structural phase transition from the insulating monoclinic ($P2_1/n$) to the metallic orthorhombic (*Pbnm*) phase, accompanied by a dramatic change in electronic properties. In the space group $P2_1/n$, the single Ni site undergoes structural disproportionation, splitting into two distinct configurations: $Ni^{(3-\delta)+}$ and $Ni^{(3+\delta)+}$.[38,39] These two NiO_6 octahedra exhibit significantly different average Ni–O bond lengths, creating an alternating pattern of contraction and expansion along all three crystallographic axes. This bond-length disproportionation directly manifests partial charge segregation on the Ni sites, with the distinct average Ni–O distances serving as a structural signature of the electronic instability.[26,40] Upon entering the metallic state (*Pbnm*), the system stabilizes in a single Ni^{3+} configuration, accompanied by uniform contraction of unit cell parameters, which is characteristic of isotropic transition metal oxides under pressure-induced metallization.[26] At 35.2 GPa, the system forms a mixed phase of *Pbnm* and $R\bar{3}c$, where the enhanced symmetry reduces lattice distortions and potentially reopens a band gap. This enables precise control of the MIT through structural distortion and orbital ordering mechanisms, thereby stabilizing the electronic transport properties against external perturbations.

Figures 2(b)–2(d) present magnified views of selected diffraction peaks, highlighting the local structural evolution under pressure. In Fig. 2(e), the interplanar spacing ratios exhibit progressively increasing separation at the critical pressures of 16.9 GPa and 35.2 GPa, reflecting systematic lattice distortion and anisotropic compression behavior. Figure 2(f) demonstrates a continuous linear reduction in unit cell volume with increasing pressure, where the observed slope changes at specific pressures provide clear evidence for phase transitions occurring within these pressure intervals. Figure 2(g) presents the Rietveld refinement patterns of the corresponding space groups under different pressures, where the gradual disappearance and merging of satellite peaks become clearly visible with increasing pressure, indicating a pressure-induced structural phase transition.[41]

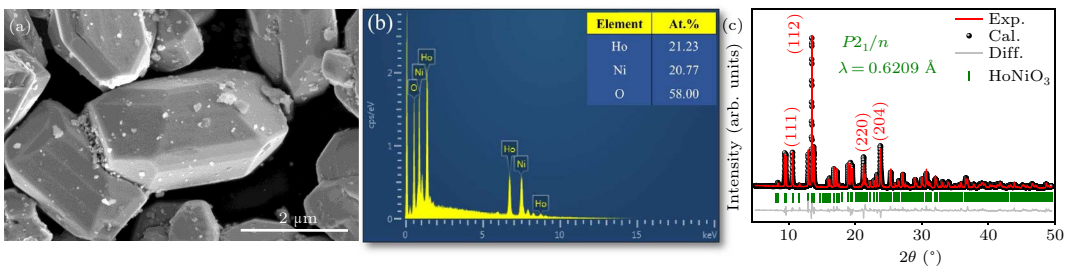


Fig. 1. Morphological and structural characterization of $HoNiO_3$ under ambient conditions. (a) SEM image with a scale bar of 2 μm, revealing well-faceted microstructures with uniform morphology. (b) EDS spectrum confirming the stoichiometric composition of Ho, Ni, and O. (c) Rietveld refinement of the synchrotron powder XRD pattern ($\lambda = 0.6209$ Å), demonstrating high phase purity and crystallinity.

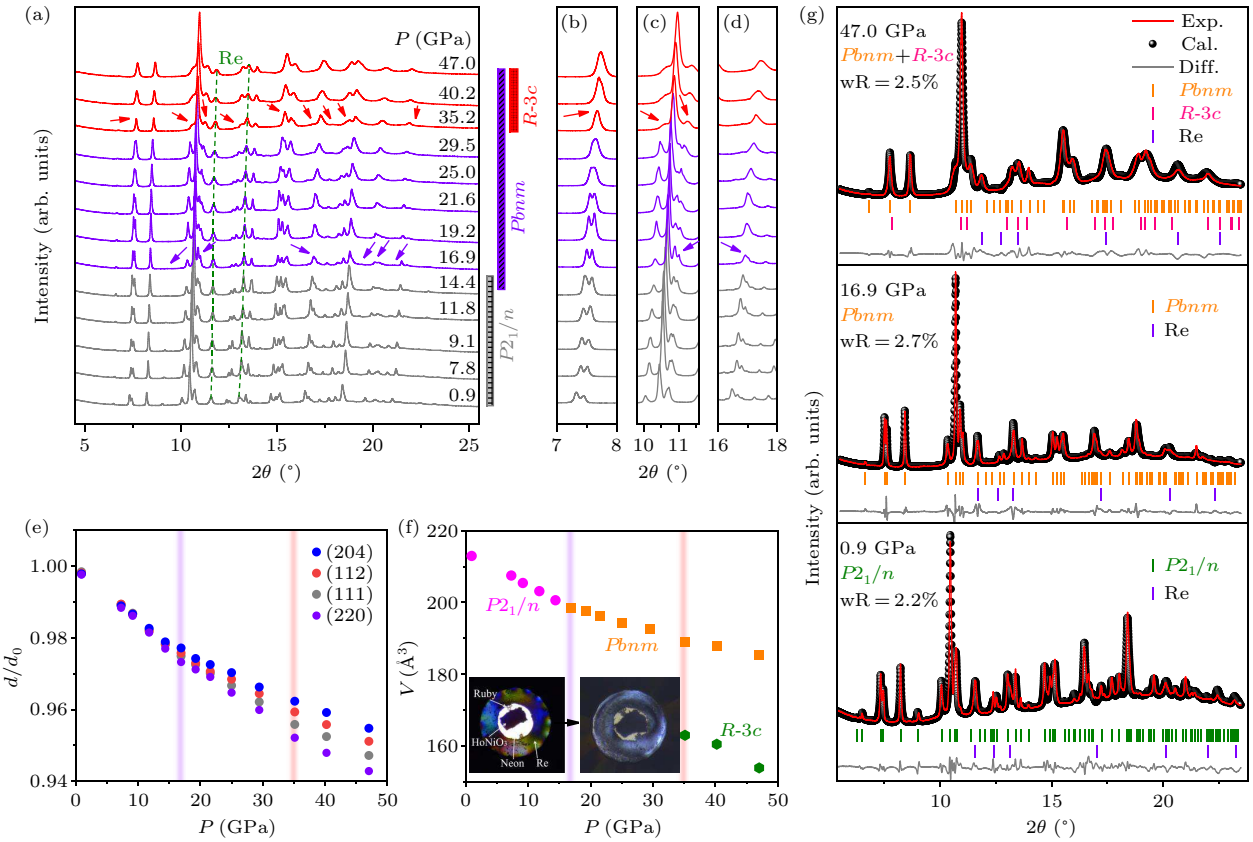


Fig. 2. Structural characterization of $HoNiO_3$ under high pressure. (a) Room-temperature synchrotron XRD patterns of $HoNiO_3$ from 0.9 GPa to 47.0 GPa in a neon atmosphere, with a wavelength of 0.4834 Å. The green dashed line indicates the shift of the Re foil peak position. (b) Enlarged view of the diffraction angle range from 7° to 8°. (c) Enlarged view of the diffraction angle range near 11°. (d) Enlarged view of the diffraction angle range from 16° to 18°. (e) Pressure dependence of the relative interplanar spacing (d/d_0) for selected crystallographic planes. (f) Relationship between pressure and the unit cell volume, with inset images showing the sample chamber before and after the measurement. (g) Rietveld refinements of the synchrotron XRD patterns at three representative pressures: the $P2_1/n$ space group at 0.9 GPa (bottom), *Pbnm* at 16.9 GPa (middle), and a mixed phase of *Pbnm* and $R\bar{3}c$ at 47.0 GPa (top).

Figure 3(a) reveals characteristic insulating behavior at 0.7 GPa and 3.2 GPa, where the system evolves from a room-temperature bad metal to a low-temperature insulator with residual conductivity. The metallic resistivity in this regime is predominantly governed by electron–phonon scattering, as evidenced by the characteristic temperature dependence of the resistivity curves.[31] Figure 3(b) shows $T_{MIT} = 174$ K under 10.3 GPa, where the low-temperature insulating phase originates from strong Coulomb repulsion between localized carriers, consistent with a Mott–Hubbard transition scenario, as evidenced by the characteristic hysteresis loop and activation energy scaling.[42] Remarkably, hydrostatic pressure induces a continuous suppression of T_{MIT}, reaching 63 K at 28.9 GPa. This pressure-driven transition bridges an antiferromagnetic insulating ground state and a paramagnetic metallic phase, revealing a direct correlation between the electronic transition and the collapse of magnetic order in the phase diagram.[43–45]

Figure 3(c) shows that at a pressure of 26.2 GPa, the electrical transport properties of $HoNiO_3$ remain strongly governed by electronic correlation effects, establishing a strongly correlated metallic state. The distinct inflection point observed in the plot delineates two regimes. In the low-temperature region (to the left of the inflection point), the significantly steeper slope of $\ln\rho$ versus $1/T$,[46] reflects enhanced temperature dependence. This behavior, extending beyond the mere suppression of electron–phonon scattering, is attributed to the dominance of strong electron–electron interactions arising from substantial on-site Coulomb repulsion, potentially coupled with residual lattice distortions from the parent insulating phase. Conversely, the high-temperature region (to the right of the inflection point) exhibits a comparatively gentler slope, signifying that the insulating state has been fully suppressed, granting electrons itinerant character and completing the pressure-induced metallization transition. Figure 3(d) reveals a metal–insulator transition at $T_{MIT} = 47$ K under 24.0 GPa. The observed discrepancy in T_{MIT} between Run 1 and Run 2 (with lower values in Run 2) originates from experimental variations, including sample thickness, inter-electrode distance, and electrode–sample contact area. Above 34.0 GPa, the pressure dependence of T_{MIT} weakens significantly, reaching 43 K at 58.0 GPa. Upon cooling, the Kondo lattice metal undergoes a transition into a narrow-gap insulating state, which may potentially host topological surface states. Concurrently, conduction electrons screen the magnetic moments of

Ho ions through the Kondo effect, forming coherent transport channels via the establishment of many-body Kondo singlets, a process dominated by strong f-electron hybridization and quantum coherence effects.[47]

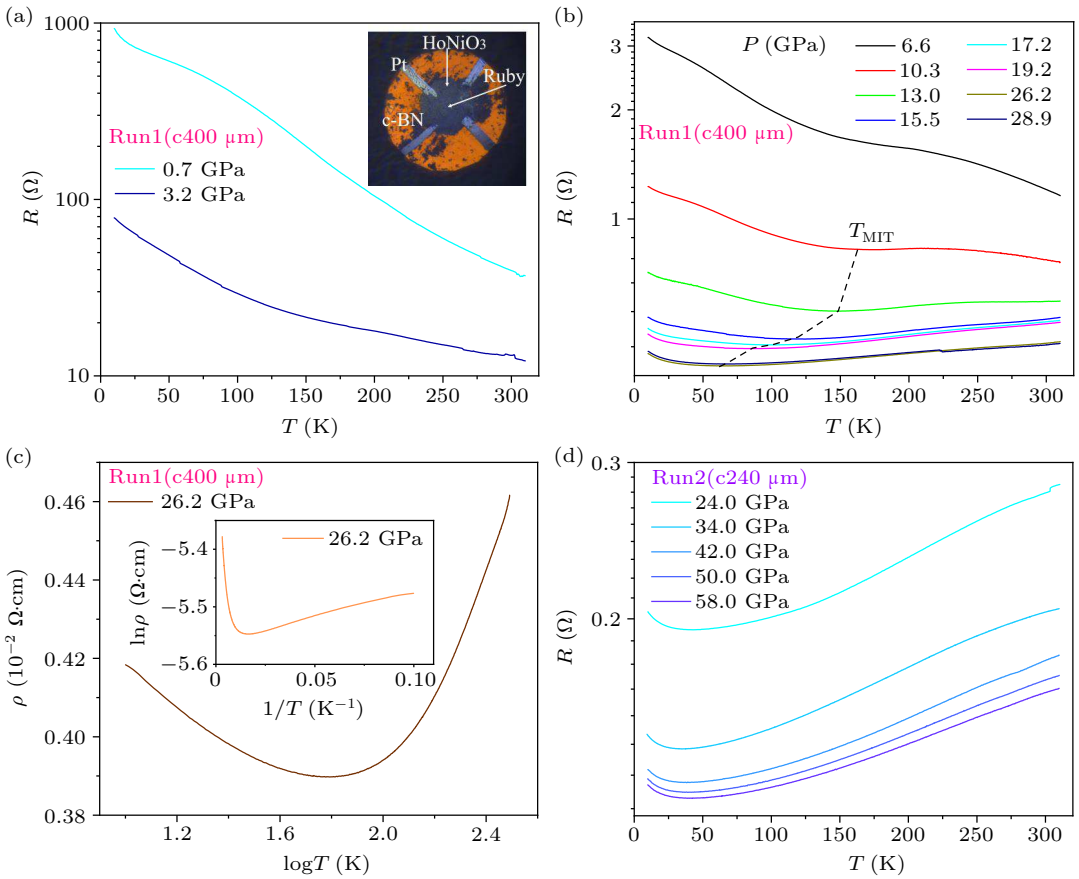


Fig. 3. Pressure-dependent electrical transport properties of $HoNiO_3$. (a) Resistance–temperature characteristic curves measured in Run 1 under DAC compression from 0.7 GPa to 3.2 GPa, showing characteristic insulating behavior. The illustration shows the use of the standard van der Pauw four-probe method in a DAC with a 400 μm diamond table. (b) *RT* characteristics from Run 1 in the 6.6–28.9 GPa range, where the black dashed line marks the pressure evolution of T_{MIT}. (c) Resistivity (ρ) as a function of $\log T$ for $HoNiO_3$ over the temperature range from 10 K to 310 K; the inset displays the curve of $\ln\rho$ versus T^{-1}. The initial thickness of the sample was 30 μm, and the estimated thickness under this pressure is 25 μm.[48] (d) High-pressure *RT* profiles from Run 2 (24.0–58.0 GPa), demonstrating the complete suppression of the insulating state at extreme pressures.

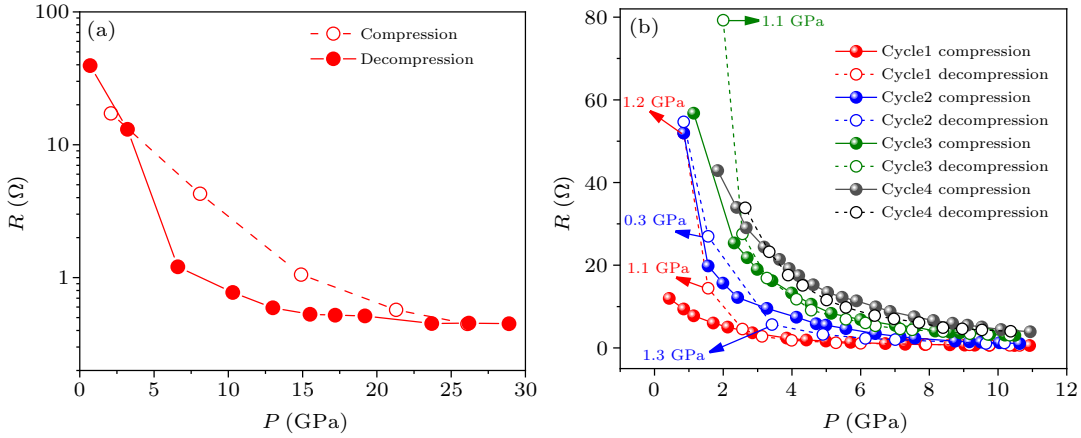


Fig. 4. Pressure-dependent resistance at room temperature. (a) Pressure dependence of resistance at 300 K extracted from Run 1. (b) Four-cycle resistance–pressure relationship of $HoNiO_3$ at room temperature (0–11 GPa). The arrows indicate the deviation between the unloading pressure (determined from the pressurization resistance–pressure curve) and the ruby pressure standard measurement.[51]

Figure 4(a) demonstrates, through decompression data, that $HoNiO_3$ exhibits remarkable reversibility, exceptional stability, and superior charge transport characteristics under extreme conditions. To evaluate potential pressure-induced fatigue or phase segregation under repeated compression–decompression cycles, Fig. 4(b) displays the pressure-dependent resistivity of $HoNiO_3$ measured over four complete compression–decompression cycles at room tempera-

ture. *Re*NiO_3 exhibits a pronounced pressure-sensitive resistivity under applied pressure, characterized by abrupt resistivity transitions with high reproducibility.[31,49] We performed systematic multi-cycle testing with in situ structural characterization, confirming the material's exceptional cycling stability without detectable degradation. The key challenge for device implementation lies in precisely controlling the transition threshold pressure while maintaining structural integrity under cyclic loading conditions.[50]

The decompression data show remarkable reversibility. The deviation between the pressure values obtained by substituting the actual pressure-release data into the exponentially fitted pressure-rise curve and the corresponding experimental unloading measurements is less than 1.5 GPa, demonstrating excellent measurement consistency and material stability. These results demonstrate that $HoNiO_3$ exhibits exceptional reversible behavior, high structural stability, and superior charge transport characteristics under extreme conditions, making it an ideal candidate for resistive sensor applications where both high sensitivity and long-term stability are critically required. With increasing cycle numbers, $HoNiO_3$ demonstrates minimal electrical resistance variation over the 6–11 GPa pressure range, along with excellent cycling stability and reproducible piezoresistive behavior, indicating significant potential for high-performance pressure sensing applications under extreme conditions.

4. Conclusion

This study systematically investigates the structural evolution and charge transport properties of $HoNiO_3$ under extreme conditions. The key scientific findings are as follows: (1) Ambient-pressure characterization using SEM microscopy, EDS elemental mapping, and XRD Rietveld refinement confirms the successful synthesis of phase-pure, well-crystallized $HoNiO_3$ polycrystals with homogeneous elemental distribution and virtually no secondary phases. (2) A sequence of pressure-induced structural transitions is observed, progressing from the monoclinic $P2_1/n$ phase to the orthorhombic *Pbnm* phase, and subsequently forming a mixed-phase regime ($Pbnm + R\bar{3}c$) under pressure. These transitions may be accompanied by distortions in Ni–O bond angles and compressive lattice contraction, reflecting the interplay between structural reorganization and electronic correlations under extreme conditions. (3) Analysis of electrical transport characteristics reveals that pressure significantly affects the resistance behavior; notably, the electrical response near T_{MIT} demonstrates the material's sensitivity to both temperature and pressure.

In summary, our findings on $HoNiO_3$ under extreme conditions provide crucial experimental insights into pressure-induced structural transitions and their implications for next-generation piezoresistive devices. The revealed complex interplay of electronic, lattice, and spin degrees of freedom in *Re*NiO_3 establishes a materials design paradigm for developing novel functional materials operating under extreme environments, with potential applications spanning quantum sensors and adaptive energy systems.

Acknowledgments

Project supported by the National Key Research and Development Program of China (Grant No. 2021YFA0718900). We thank the Shanghai Synchrotron Radiation Facility BL17UM (https://cstr.cn/31124.02.SSRF.BL17UM) for assistance with HPXRD measurements.

References

[1] Jaramillo R, Ha S D, Silevitch D M and Ramanathan S 2014 *Nat. Phys.* **10** 304
[2] Middey S, Chakhalian J, Mahadevan P, Freeland J W, Millis A J and Sarma D D 2016 *Annu. Rev. Mater. Res.* **46** 305
[3] Constantin L A, Fabiano E and Della Sala F 2018 *Phys. Rev. B* **97** 205137
[4] Mercy A, Bieder J, Iniguez J and Ghosez P 2017 *Nat. Commun.* **8** 1677
[5] Zhang X, Jiang J, Shen Z, Dan Z, Li M, Lin Y, Nan C W, Chen L and Shen Y 2018 *Adv. Mater.* **30** 1707269
[6] Mazin I I, Khomskii D I, Lengsdorf R, Alonso J A, Marshall W G, Ibberson R M, Podlesnyak A, Martínez-Lope M J and Abd-Elmeguid M M 2007 *Phys. Rev. Lett.* **98** 176406
[7] Torrance J B, Lacorre P, Nazzal A I, Ansaldo E J and Niedermayer C 1992 *Phys. Rev. B* **45** 8209
[8] Prakapenka V B, Kubo A, Kuznetsov A, Laskin A, Shkurikhin O, Dera P, Rivers M L and Sutton S R 2008 *High Pressure Res.* **28** 225
[9] Chen B J, Sun Y, Yang N, Zhong N, Zhang Y Y, Bai W, Sun L, Tang X D, Yang P X, Xiang P H and Duan C G 2017 *J. Phys. D: Appl. Phys.* **50** 235302
[10] Rodrigues J E, Rosa A, Garbarino G, Irifune T, Martínez J L, Alonso J A and Mathon O 2023 *Chem. Mater.* **35** 5079
[11] Chen J, Mao W, Ge B, Wang J, Ke X, Wang V, Wang Y, Dobeli M, Geng W, Matsuzaki H, Shi J and Jiang Y 2019 *Nat. Commun.* **10** 694
[12] Klein Y M, Kozłowski M, Linden A, Lacorre P, Medarde M and Gawryluk D J 2021 *Cryst. Growth Des.* **21** 4230
[13] Hao D, Chai R, Liang L, Xia L, Wang Z and Liu P 2022 *Phys. Eng.* **32** 121
[14] Fernández-Díaz M T, Alonso J A, Martínez-Lope M J, Casais M T and García-Muñoz J L 2001 *Phys. Rev. B* **64** 144417
[15] Wang X, Khachai H and Khenata R 2019 *Superlattices Microstruct.* **130** 472
[16] Neupane M, Alidoust N, Xu S Y, Kondo T, Ishida Y, Kim D J, Liu C, Belopolski I, Jo Y J, Chang T R, Jeng H T, Durakiewicz T, Balicas L, Lin H, Bansil A, Shin S, Fisk Z and Hasan M Z 2013 *Nat. Commun.* **4** 2991
[17] Hepting M 2016 *Ordering Phenomena in Nickelate Heterostructures Studied by Elastic and Inelastic Photon Scattering* (Ph.D. Dissertation) (Stuttgart: Universität Stuttgart)
[18] Ardizzone I 2021 *An Optical Study of the Physics of the Rare Earth Nickelates* (Ph.D. Dissertation) (Switzerland: University of Geneva)
[19] Amboage M, Hanfland M, Alonso J A and Martínez-Lope M J 2005 *J. Phys.: Condens. Matter* **17** S783
[20] Cheng J G, Zhou J S, Goodenough J B, Alonso J A and Martinez-Lope M J 2010 *Phys. Rev. B* **82** 085107
[21] Zhou J S, Goodenough J B and Dabrowski B 2004 *Phys. Rev. B* **70** 081102
[22] Hampel A, Liu P, Franchini C and Ederer C 2019 *NPJ Quantum Mater* **4** 5
[23] Lengsdorf R G 2005 *Interplay Between Transport, Magnetism and Structural Properties of Transition Metal Oxides under High Pressure* (Ph.D. Dissertation) (Germany: Universität zu Köln)
[24] Garcia-Munoz J L, Rodriguez-Carvajal J, Lacorre P and Torrance J B 1992 *Phys. Rev. B* **46** 4414

[25] Rodríguez-Carvajal J, Rosenkranz S, Medarde M, Lacorre P, Fernandez-Díaz M T, Fauth F and Trounov V 1998 *Phys. Rev. B* **57** 456

[26] Alonso J A, Martínez-Lope M J, Casais M T, García-Muñoz J L, Fernández-Díaz M T and Aranda M A G 2001 *Phys. Rev. B* **64** 094102

[27] Takagi H and Hwang H Y 2010 *Science* **327** 1601

[28] Schlappa J, Wohlfeld K, Zhou K J, Mourigal M, Haverkort M W, Strocov V N, Hozoi L, Monney C, Nishimoto S, Singh S, Revcolevschi A, Caux J S, Patthey L, Ronnow H M, van den Brink J and Schmitt T 2012 *Nature* **485** 82

[29] Sun L, Wu Q, Cai S, Ding Y and Mao H K 2024 *Matter Radiat. Extremes* **9** 043001

[30] Imada M, Fujimori A and Tokura Y 1998 *Rev. Mod. Phys.* **70** 1039

[31] Cui Y, Gao J, Dong H, Li Z, Zhang Z, Wang V, Nie K, Zeng Z, Jiang Y, Chen N, Mao H K and Chen J 2024 *J. Phys. Chem. Lett.* **15** 7716

[32] Prescher C and Prakapenka V B 2015 *High Pressure Res.* **35** 223

[33] Sun H, Huo M, Hu X, Li J, Liu Z, Han Y, Tang L, Mao Z, Yang P, Wang B, Cheng J, Yao D X, Zhang G M and Wang M 2023 *Nature* **621** 493

[34] Boyang F, Wenfeng Z, Fuyang L, Luhong W, Haozhe L, Sheng-Ping G and Weizhao C 2025 *Chin. Phys. B* **34** 086102

[35] Xiaoxin W, Yingjian W, Siqi L, Juncheng L, Jingshu W, Lihua Y, Qi Z, Yanqing L, Junkai Z and Hongsheng J 2024 *Chin. Phys. B* **33** 056201

[36] García-Muñoz J L, Amboage M, Hanfland M, Alonso J A, Martínez-Lope M J and Mortimer R 2004 *Phys. Rev. B* **69** 094106

[37] Ye H, Hua E, Xu F, Lu J, Jin F, Wu W, Si L and Wang L 2024 *Chin. Phys. Lett.* **41** 117301

[38] Alonso J A, Martínez-Lope M J, Casais M T, García-Muñoz J L and Fernández-Díaz M T 2000 *Phys. Rev. B* **61** 1756

[39] Ramos A Y, Piamonteze C, Tolentino H C N, Souza-Neto N M, Bunau O, Joly Y, Grenier S, Itié J P, Massa N E, Alonso J A and Martinez-Lope M J 2012 *Phys. Rev. B* **85** 045102

[40] Pratontep S, Brinkmann M, Nüesch F and Zuppiroli L 2004 *Synth. Met.* **146** 387

[41] Yiping G, Chenchen L, Can T, Chengcheng Z, Xiaoli H and Tian C 2024 *Chin. Phys. B* **33** 126104

[42] Mott N F 1949 *Proc. Phys. Soc. A* **62** 416

[43] Ye H, Hua E, Xu F, Lu J, Jin F, Wu W, Si L and Wang L 2024 *Chin. Phys. Lett.* **41** 117301

[44] Scagnoli V, Staub U, Janousch M, Mulders A M, Shi M, Meijer G I, Rosenkranz S, Wilkins S B, Paolasini L, Karpinski J, Kazakov S M and Lovesey S W 2005 *Phys. Rev. B* **72** 155111

[45] Hampel A 2019 *Interplay Between Structural, Electronic, and Magnetic Properties in Rare-Earth Nickelates* (Ph.D. Dissertation) (Switzerland: ETH Zurich)

[46] Zhang Y, Su D, Huang Y, Shan Z, Sun H, Huo M, Ye K, Zhang J, Yang Z, Xu Y, Su Y, Li R, Smidman M, Wang M, Jiao L and Yuan H 2024 *Nat. Phys.* **20** 1269

[47] Huang X, Zhang H, Li J, Huo M, Chen J, Qiu Z, Ma P, Huang C, Sun H and Wang M 2024 *Chin. Phys. Lett.* **41** 127403

[48] Huang X, Gao C, Han Y, Li M, He C, Hao A, Zhang D, Yu C, Zou G and Ma Y 2007 *Appl. Phys. Lett.* **90** 242102

[49] Chen C, Zhou Y, Chen X, Han T, An C, Zhou Y, Yuan Y, Zhang B, Wang S, Zhang R, Zhang L, Zhang C, Yang Z, DeLong L E and Cao G 2020 *Phys. Rev. B* **101** 144102

[50] Wu J, Feng Y, Ren Y, Zhang Z, Yang Y, Wang X, Su F, Dong H, Lu Y, Zhang X, Deng Y, Xiang B and Chen Z 2024 *J. Chem. Phys.* **160** 034707

[51] Goettel K A, Mao H K and Bell P M 1985 *Rev. Sci. Instrum.* **56** 1420